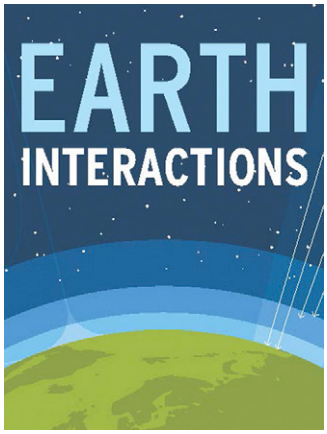

Climate Drivers Linked to Changing Seasonality of Alaska Coastal Tundra Vegetation Productivity

Peter A. Bieniek,[*,+,#] Uma S. Bhatt,[+] Donald A. Walker,[@] Martha K. Raynolds,[@] Josefino C. Comiso,[&] Howard E. Epstein,[**] Jorge E. Pinzon,[++] Compton J. Tucker,[++] Richard L. Thoman,[##] Huy Tran,[+,@@] Nicole Mölders,[+] Michael Steele,[&&] Jinlun Zhang,[&&] and Wendy Ermold[&&]

[+] Geophysical Institute and Department of Atmospheric Sciences, University of Alaska Fairbanks, Fairbanks, Alaska
[#] International Arctic Research Center, University of Alaska Fairbanks, Fairbanks, Alaska
[@] Institute of Arctic Biology and Department of Biology and Wildlife, University of Alaska Fairbanks, Fairbanks, Alaska
[&] Cryospheric Sciences Branch, NASA Goddard Space Flight Center, Greenbelt, Maryland
[**] Department of Environmental Sciences, University of Virginia, Charlottesville, Virginia
[++] Biospheric Sciences Branch, NASA Goddard Space Flight Center, Greenbelt, Maryland
[##] NOAA/National Weather Service, Alaska Region, Fairbanks, Alaska
[@@] Bingham Entrepreneurship and Energy Research Center, Utah State University, Vernal, Utah
[&&] Polar Science Center, Applied Physics Laboratory, University of Washington, Seattle, Washington

Received 3 February 2015; in final form 18 September 2015

[*] Corresponding author address: Peter A. Bieniek, 930 Koyukuk Dr., P.O. Box 757340, Fairbanks, AK 99775.
E-mail address: pbieniek@alaska.edu

DOI: 10.1175/EI-D-15-0013.1

ABSTRACT: The mechanisms driving trends and variability of the normalized difference vegetation index (NDVI) for tundra in Alaska along the Beaufort, east Chukchi, and east Bering Seas for 1982–2013 are evaluated in the context of remote sensing, reanalysis, and meteorological station data as well as regional modeling. Over the entire season the tundra vegetation continues to green; however, biweekly NDVI has declined during the early part of the growing season in all of the Alaskan tundra domains. These springtime declines coincide with increased snow depth in spring documented in northern Alaska. The tundra region generally has warmed over the summer but intraseasonal analysis shows a decline in midsummer land surface temperatures. The midsummer cooling is consistent with recent large-scale circulation changes characterized by lower sea level pressures, which favor increased cloud cover. In northern Alaska, the sea-breeze circulation is strengthened with an increase in atmospheric moisture/cloudiness inland when the land surface is warmed in a regional model, suggesting the potential for increased vegetation to feedback onto the atmospheric circulation that could reduce midsummer temperatures. This study shows that both large- and local-scale climate drivers likely play a role in the observed seasonality of NDVI trends.

KEYWORDS: Geographic location/entity; Arctic; Land surface; Atmosphere−ocean structure/phenomena; Vegetation; Physical Meteorology and Climatology; Climate variability

1. Introduction

Many climatic changes have been documented in the Arctic summer over the satellite record and at longer time scales, most notably increasing surface air temperatures and a decline in sea ice (Berner et al. 2005; Melillo et al. 2014). These climatic variations are especially pronounced in the Arctic due to the role of polar amplification (Bekryaev et al. 2010; Serreze and Barry 2011), which is caused primarily by decreasing sea ice cover. The decline in sea ice has had far-reaching terrestrial consequences not only for the climate but also for vegetation and other biota in the Arctic (Bhatt et al. 2010; Dutrieux et al. 2012; Macias-Fauria et al. 2012; Bhatt et al. 2014). Tundra vegetation throughout Alaska and the Arctic has largely been greening over the satellite record (1982–2013), and the vegetation productivity rise has been linked to increased summer warmth (Jia et al. 2003; Walker et al. 2003) resulting from sea ice retreat (Bhatt et al. 2010; Dutrieux et al. 2012). The Advanced Very High Resolution Radiometer (AVHRR)-derived normalized difference vegetation index (NDVI) (Pinzon and Tucker 2014) provides a long-term dataset of remotely sensed vegetation productivity, which is correlated with aboveground biomass in the Arctic (Shippert et al. 1995; Jia et al. 2003; Walker et al. 2003; Raynolds et al. 2004, 2012; Epstein et al. 2012). However, updated NDVI trends do not show simple secular increases everywhere despite continued sea ice decline and general warming (Bhatt et al. 2013).

The Alaskan coastal tundra region is controlled by the cool summer air mass associated with the location of the sea ice (Conover 1960; Cantlon 1961; Haugen and Brown 1980; Yurtsev 1994; Zhang et al. 1996; Epstein et al. 2004). Therefore, as Arctic sea ice has declined and surface temperatures have warmed, it is not surprising that the tundra vegetation responded with greening. Climate model simulations forced only by reduced Arctic sea ice support the notion that decreased summer sea ice warms nearby coastal air temperatures (Bhatt et al. 2008; Lawrence et al. 2008).

While precipitation amounts are small in the Arctic, the soils tend to be moist due to the permafrost layer limiting the downward flow of water, and tundra plants are primarily temperature limited as a result. The air is also moist due to the moisture available from the adjacent Arctic Ocean, especially when it is ice free. With the decline in sea ice, summer temperatures are not as constrained by the cold, high albedo surface of the ice and can more readily increase with available solar insolation. The decline in Arctic sea ice has led to enhanced summer warmth and increased plant productivity on the broad pan-Arctic scale but not necessarily at the local scale.

Alaska's climate variations and trends vary regionally, which can affect the spatial patterns of vegetation productivity. The Beaufort and east Chukchi coastal tundra regions (Figure 1a) are bounded to the south by the Brooks Range and the Arctic Ocean to the north while the east Bering region is located farther to the south along the Bering Sea near the Pacific Ocean. A narrow portion of the Beaufort tundra region also extends into Canada along the Beaufort Sea coast. These three tundra regions are located in the North Slope (Beaufort and east Chukchi) and the West Coast (east Chukchi and east Bering) Alaska climate divisions. The Alaskan climate divisions delineate geographical regions with similar climate variability and are a convenient tool to regionalize variability and trends (Bieniek et al. 2012). The North Slope division has experienced a significant increase in annual surface air temperature and precipitation over the last 30 years with much of the warming and wetting concentrated in late summer and fall, while the West Coast division has experienced much weaker and more mixed trends over the same period (Bieniek et al. 2014). The North Slope region is also quite dry relative to other coastal areas in Alaska and experiences 24 h of daylight in summer and night in winter (Shulski and Wendler 2007).

Trends for the Alaskan coastal tundra zone over 1982–2013 are presented in Figures 1b–d for spring sea ice, summer open water, summer warmth index [sum of monthly average temperatures above freezing (SWI)], maximum annual NDVI (maxNDVI), and time-integrated NDVI (TI-NDVI is the sum of biweekly maximum NDVI). There is increased open water along coastal Alaska (Figures 1b,c) and earlier (later) spring sea ice breakup adjacent to the northern (southern) Alaskan tundra (Figure 1d). SWI has overall increased; however, the addition of recent summers shows increasing areas with weak positive or even negative trends (Figure 1d) in Alaska as well as for the pan-Arctic (Bhatt et al. 2013). Tundra vegetation greening has continued and even strengthened in northern Alaska, while browning or declining vegetation trends have continued for southwestern Alaska (Figures 1b,c), relative to previous studies of northern (Jia et al. 2003) and southwestern Alaska (Verbyla 2008; Bhatt et al. 2010). The greening trend in the northern portion of Alaska has been in part attributed to an increase in shrubs (Sturm et al. 2001; Tape et al. 2006), and this region has experienced an increased growing season length (Jia et al. 2003; Xu et al. 2013). The browning trend in southwestern Alaska in the inland boreal forest regions has been attributed to increased drought stress and insect infestation (Parent and Verbyla 2010; Beck et al. 2011); however, the precise mechanism related to the browning of the coastal tundra is unclear.

This study evaluates the potential climate drivers of changes in vegetation seasonality (i.e., change in the seasonal cycle/progression or intra-annual variations) using remote sensing data in conjunction with meteorological station data (Figure 1a), atmospheric reanalyses, and a regional model for three coastal tundra regions in Alaska. We first analyze the seasonality of the climatology and trends of sea ice concentration, ocean heat content, land surface temperatures, biweekly

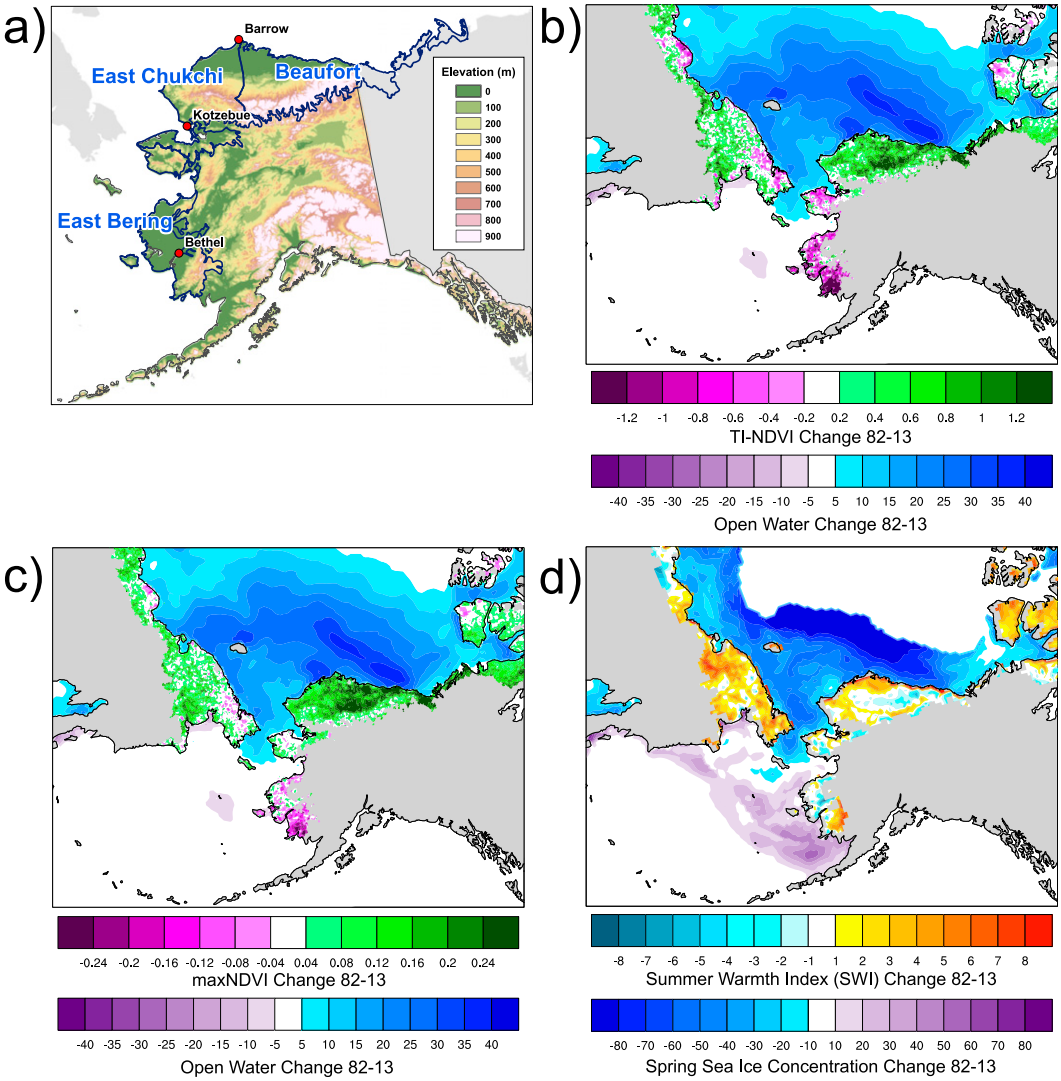

Figure 1. The names and outlines (a) of the three Treshnikov regions (black lines) along with weather observation stations used in this study and topography of Alaska, trend magnitude change for 1982–2013 based on a linear trend of (b) TI-NDVI (unitless) and May–August open water (%), (c) seasonal maxNDVI (unitless) and May–August open water (%), and (d) magnitude of change in sea ice breakup (as represented by 50% sea ice concentration) and summer warmth index (°C month). TI-NDVI and maxNDVI trends are significant at the 95% or greater level for most of the Beaufort, while less so for the east Chukchi and east Bering. The summer warmth index has few significant trends at the 95% or greater level except for along the northern coastline. The declines in spring sea ice concentration are significant at the 95% or greater level throughout the Beaufort and east Chukchi Seas, while the increases in the east Bering are not statistically significant. The increased open-water trends over the Beaufort Sea are statistically significant at the 95% or greater level, while those in the east Chukchi and east Bering are not.

NDVI, and snow water equivalent. The unique aspect of this study includes the synthesis of various climate datasets to identify mechanisms associated with trends in the seasonality of summer tundra vegetation productivity and land surface temperatures in Alaska.

2. Data and methods

The three tundra regions used in this analysis follow those utilized in Bhatt et al. (2010). They were based on the ocean regions outlined by Treshnikov (1985) and modified using floristic provinces from Walker et al. (2005). The tundra domains employed in this study will be named for the contiguous seas, namely, east Bering, east Chukchi, and Beaufort, and represent the areas of coastal tundra regions as well as nearby ocean domains (Figure 1a). The statistical significance of correlations and trends was assessed using a two-tailed Student's *t* test at the 95% and 90% levels. Climate data in Alaska and the Arctic contain multidecadal variability along with trends (Polyakov et al. 2013); therefore, the degrees of freedom used in the trend significance tests were adjusted based on the lag-1 autocorrelation method outlined by Santer et al. (2000). All trends presented were computed by least squares regression, and trend magnitude change was then computed by multiplying the slope of the trend line by the number of years in the time series. The terms trend and magnitude change will be used interchangeably in this study and will refer to the trend magnitude change.

2.1. Remotely sensed data

The normalized difference vegetation index is defined as NDVI = (NIR − VIS)/(NIR + VIS), where NIR is the surface reflectance of near-infrared radiation (0.725−1.1 μm) and VIS is the reflectance of visible radiation (0.55–0.70 μm) (Deering 1978; Tucker 1979). NDVI is a proxy for vegetation productivity, integrates numerous photosynthetic factors related to ecosystem structure and function, ranges from zero (i.e., no vegetation activity) to one and is unitless. The amount of radiation absorbed by the plants primarily depends on the physical properties of the vegetation including the species, the vertical and horizontal structure, phenological stage, and the physiological condition. This study employs the Global Inventory Modeling and Mapping Studies 3rd Generation (GIMMS3g) NDVI dataset, which is derived from the wavelength bands retrieved from the AVHRR sensors 1982–2013 (Pinzon and Tucker 2014). The maxNDVI is the highest summer NDVI value, which represents the seasonal peak green biomass. TI-NDVI is the sum of biweekly values above a threshold of 0.05 during the growing season from May to September. TI-NDVI incorporates the length of the growing season and represents gross primary production (Tucker and Sellers 1986). In addition, TI-NDVI is more strongly correlated than maxNDVI to climate parameters such as spring sea ice cover and tundra land surface temperatures (Bhatt et al. 2010). In this study, the maximum NDVI in each biweekly period (hereafter biweekly NDVI) is used to investigate the seasonality of NDVI change.

This analysis used weekly sea ice concentration derived from Special Sensor Microwave Imager (SSM/I) data (Comiso and Nishio 2008) and AVHRR radiometric surface temperature from 1982 to 2013. The area average sea ice concentration was

calculated within a 100-km buffer of the coast of each tundra region. The AVHRR surface temperature data have been enhanced through more effective cloud masking techniques and calibration through the utilization of in situ surface temperature data (Comiso 2003). Monthly AVHRR land surface temperatures served to calculate the SWI, which is the sum of May–September monthly average land surface temperatures greater than 0°C, while the weekly temperature data were used to examine the seasonality of trends and variability.

2.2. Reanalysis and meteorological station data

Snow water equivalent (SWE) data were obtained from the European Space Agency (ESA)'s Global Snow Monitoring for Climate Research (GlobSnow) at a daily resolution on a 25-km Equal-Area Scalable Earth (EASE) grid for the period 1982–2013 (Takala et al. 2011). GlobSnow assimilates passive microwave–derived SWE with station snow depth to form a consistent product. Weekly SWE was then calculated to match the weeks of the sea ice and surface temperature data for ease of comparison.

Biweekly ocean heat content data were derived from the Pan-Arctic Ice Ocean Modeling and Assimilation System (PIOMAS) dataset (Steele et al. 2011) for 1988–2013, in which sea surface temperature and sea ice concentration were assimilated into the model simulation. The value of heat content is a vertical integration from the surface to 100-m depth or the bottom if shallower. The heat content was calculated by vertically integrating the density of the ocean times the specific heat capacity times the ocean potential temperature minus a reference temperature of −2°C. The data were then area averaged within a 100-km buffer of the coast of each tundra region.

Mean sea level pressure (SLP) data were obtained from the NCEP–NCAR Reanalysis 1 (Kalnay et al. 1996) at daily temporal and 2.5° spatial resolution for 1982–2013. Weekly SLP were then calculated based on the weeks used by the sea ice and surface temperature datasets for ease of comparison.

Station cloud cover data were obtained for Barrow, Kotzebue, and Bethel (locations shown in Figure 1a) from the integrated surface database (ISD; available online at http://www.ncdc.noaa.gov/oa/climate/isd/index.php) for 1982–2013.

2.3. Regional model

To assess the linkages between temperatures over the Beaufort and east Chukchi tundra regions and the local atmospheric circulation and processes, idealized experiments utilizing the Weather Research and Forecasting (WRF) Model (Skamarock et al. 2008) were conducted in one-way coupled mode. Use of a model study in the Beaufort region is particularly advantageous due to the particularly sparse network of observation stations in northern Alaska. The parent model domain encompassed Siberia, the Arctic Ocean, and Alaska with a 25-km grid increment and the North Slope and Chukchi and Beaufort Seas with a 5-km grid increment. Cloud microphysical processes followed the WRF Model single-moment 6-class scheme (Hong and Lim 2006). Subgrid-scale cloud convection was treated by the improved Grell 3D ensemble scheme (Grell and Dévényi 2002). The Rapid Radiative Transfer Model (Mlawer et al.

1997) was employed to calculate longwave radiation for multiple bands, trace gases, and cloud microphysical species. The Goddard two-stream multiband scheme with ozone from climatology and cloud species was applied for shortwave radiation (Chou and Suarez 1994). The Eta Model surface layer and atmospheric boundary layer models (Janjić 2002) were used. The exchange of heat, matter, and momentum at the surface–atmosphere interface were described by the unified Noah land surface scheme (Tewari et al. 2004). Boundary forcing and initialization data were provided by the National Centers for Environmental Prediction global final analysis and the WRF Model was initialized every 5 days.

A reference simulation was run over the June–July 2010 period (the year was randomly selected), and a positive 3°C anomaly was then added to the surface temperature of the reference simulation over the Beaufort region (see Figure 1a) only. The warm anomaly simulation was then run for the same period as the reference but with the specified surface temperatures. A similar cold anomaly simulation was also integrated for comparison but will not be presented, as the warm anomaly response is the focus of this study. A 3°C anomaly is greater than two standard deviations of the daily average temperatures in northern Alaska and was applied to enhance the response. Therefore, it is likely an exaggeration of past or future observed change.

3. Results and discussion

3.1. Seasonality of trends

While the Beaufort and east Chukchi regions are adjacent to areas of sea ice loss in the Arctic Ocean in spring and summer, the east Bering displays increased sea ice in spring (Figure 1d). The annual cycle of the weekly climatology (Figure 2) shows that the longest ice-free season occurs in the east Bering, while the more northerly zones may have some sea ice present in summer. The most striking trends are in the Beaufort and east Chukchi regions (Figures 2a,b) in August–November with the steepest weekly declines occurring in the Beaufort over 1982–2013. Declines, although weaker, have also occurred in spring. These sea ice declines are not uniform throughout the Beaufort Sea and have been linked with reduced import of multiyear sea ice from the Canadian Arctic Archipelago into the western Beaufort Sea (Steele et al. 2015). These results indicate a longer ice-free season in the Beaufort and east Chukchi sea zones. The trends in the east Bering are mostly increases in December–April (Figure 2c), and there have even been positive trends in sea ice concentration in April–May in recent decades, consistent with the spatial pattern in Figure 1d suggesting delayed onset of breakup. The winter increase in Bering Sea ice concentration has been linked to a persistent atmospheric circulation by Matthewman and Magnusdottir (2011) and is not inconsistent with the overall Arctic sea ice decline since this is a seasonally ice covered area, where ice formation is a function of the local atmospheric circulation. Coastal sea ice melts earlier in spring and freezes later in the fall in the Beaufort and east Chukchi regions, extending the open-water season in northern Alaska. In the east Bering region, the coastal sea ice has been melting later in spring but still melts before tundra vegetation greens up.

The trends in sea ice set the stage for the changes that have occurred in ocean heat content over the three regions (Figure 3). The seas adjacent to the three tundra

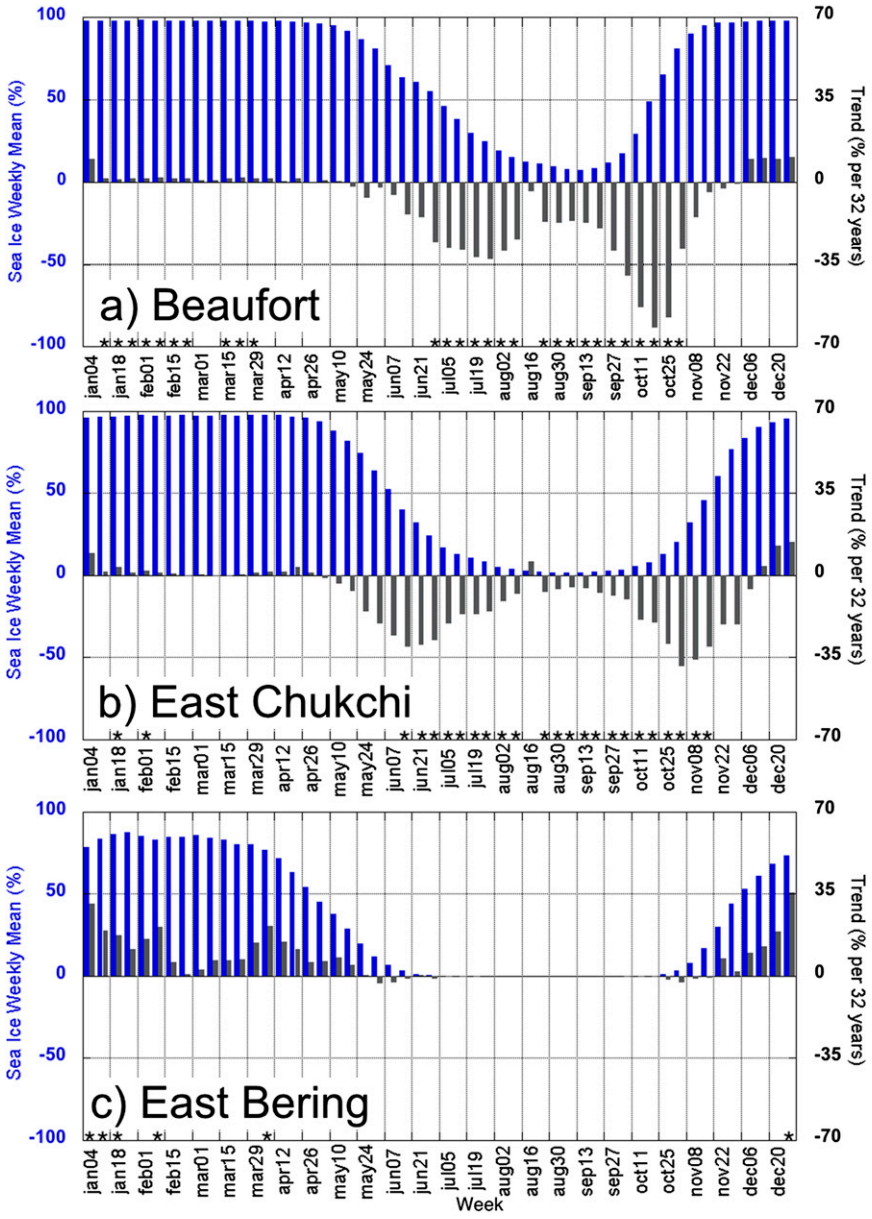

Figure 2. Weekly sea ice concentration climatology (blue) and trend magnitude change 1982–2013 (dark gray) for the (a) Beaufort, (b) east Chukchi, and (c) east Bering tundra regions. Weekly periods with trends significant at the 95% or greater level are marked with an asterisk on the *x* axis.

regions experience their climatological maximum in ocean heat content when sea ice is at its minimum in August (cf. Figures 2 and 3). The Beaufort and east Chukchi have experienced increased ocean heat content (Figures 3a,b) over the record corresponding to their sea ice reduction. Similarly, the east Bering has experienced reduced ocean heat content (Figure 3c) corresponding to increased sea ice in spring. Heat content trends in the Beaufort region display a seasonal cycle that follows the

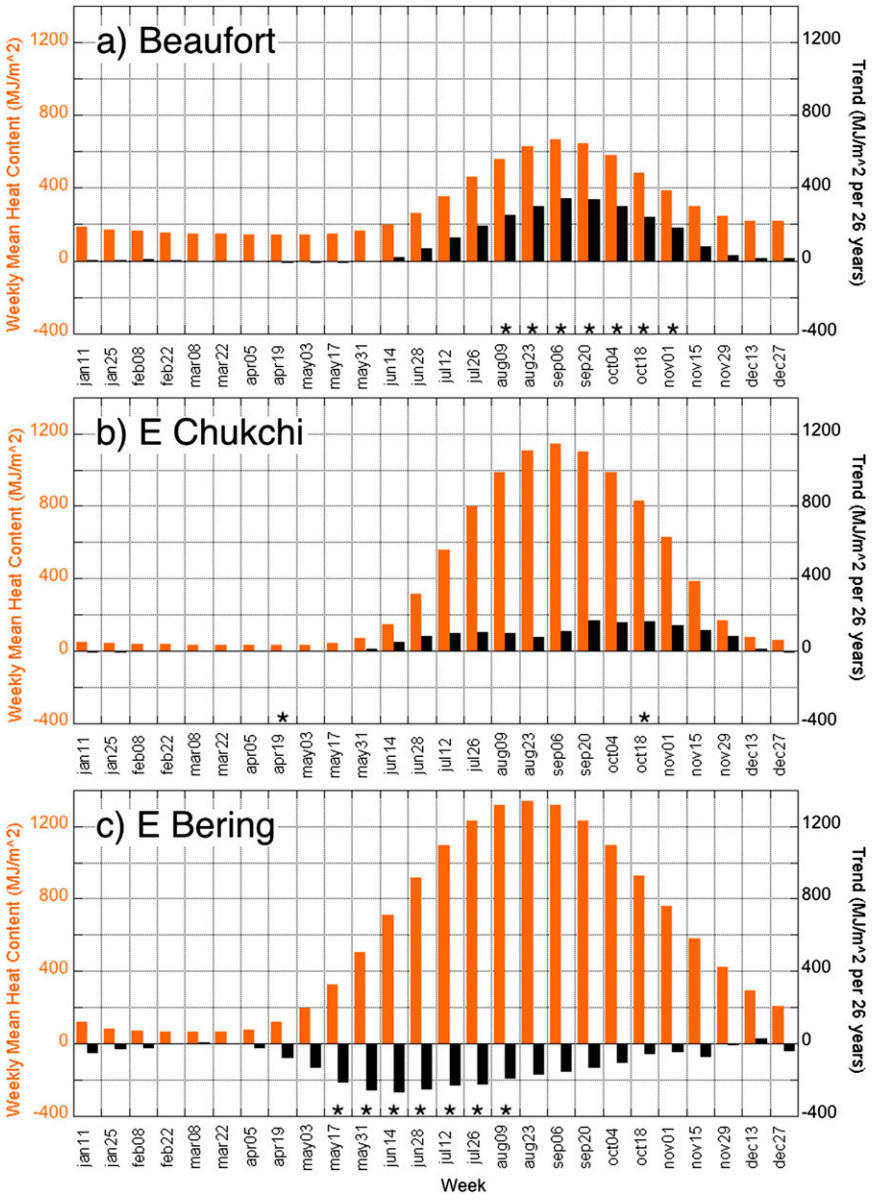

Figure 3. Biweekly total column ocean heat content climatology (orange) and trend magnitude change 1988–2013 (dark gray) within 100 km of the coast of the (a) Beaufort, (b) east Chukchi, and (c) east Bering tundra regions. Biweekly periods with trends significant at the 95% or greater level are marked with an asterisk on the *x* axis.

climatological mean of heat content, with the largest positive trends in early September. Trends in the east Chukchi have a similar magnitude from June to November when heat content is climatologically largest. East Bering heat content displays the largest negative trends in early summer (i.e., mid-June) when the climatological heat content is increasing from the January–March minimum values.

SWI has generally increased for all three tundra regions; however, there are mixed trends spatially (Figure 1d). When evaluating the seasonality of the trends in weekly surface temperature, mixed trends are found throughout the year in all three regions (Figure 4). All share cooling trends in recent decades in much of the winter and spring. They also experienced warming trends in parts of May–June and August corresponding to the decline in sea ice, and the trends are most notable in the Beaufort and east Chukchi regions. All three regions share a slight cooling trend in portions of June–July. These regions had previously had general warming trends in summer (e.g., Bhatt et al. 2010), and it appears that those trends have now weakened and even switched sign to slight cooling. Weakened warming trends and even cooling in summer have been noted in the Arctic starting in the late 1990s to early 2000s (e.g., Manabe et al. 2011; Bhatt et al. 2013, 2015, manuscript submitted to *Environ. Res. Lett.*), and the midsummer cooling trends in the three Alaskan tundra regions are consistent with those observations. Similar weak cooling trends were also found in reanalysis surface air temperature data in areas of northern and western Alaska in midsummer (not shown). This recent cooling during the peak of the summer season (June–July) suggests that the response to sea ice decline is not simply increased warming but rather that other processes are playing a role in temperature variations.

NDVI increased over 1982–2013 for both TI-NDVI (Figure 1b) and maxNDVI (Figure 1c) in the Beaufort and east Chukchi regions, while declines occurred over the southern east Bering region. The biweekly trends of NDVI reflect the generally positive seasonal trends (Figure 5). However, there are early season declines over the period in the Beaufort and east Chukchi regions in contrast to their overall seasonal increase. The Beaufort region (Figure 5a) has seen the strongest trends of the three Alaskan tundra regions with the positive NDVI trends occurring during the period of peak climatological maxNDVI. Trends for the east Chukchi NDVI (Figure 5b) are quite similar to those of the Beaufort but weaker. The east Bering (Figure 5c) deviates from the other two regions in that there has been an overall decline in biweekly NDVI throughout the summer with the largest decline occurring in May. The east Bering region also has NDVI greater than zero throughout the year, as it is maritime tundra where there are often snow-free conditions in winter and vegetation is exposed. The large negative biweekly NDVI trends in May–June are consistent with the delayed breakup of sea ice in the adjoining sea and generally cooler ocean temperatures. However, since there is a gap between sea ice melt and greenup, this suggests that other processes such as the timing of snowmelt, winter snow-free events, and so on, need to be considered.

3.2. Role of snow in spring NDVI declines

Snow water equivalent, which is related to snow depth, is a likely driver of the observed spring NDVI declines as snow impacts vegetation in several ways. The timing of melt determines when plants may begin to photosynthesize and grow, while snow depth can influence the amount of water available for the plants in the Arctic summer (Walker et al. 2001). The insulating effects of snow can also influence the freeze and thaw of the active layer in permafrost areas (Zhang 2005). The active layer impacts plants as it determines the space

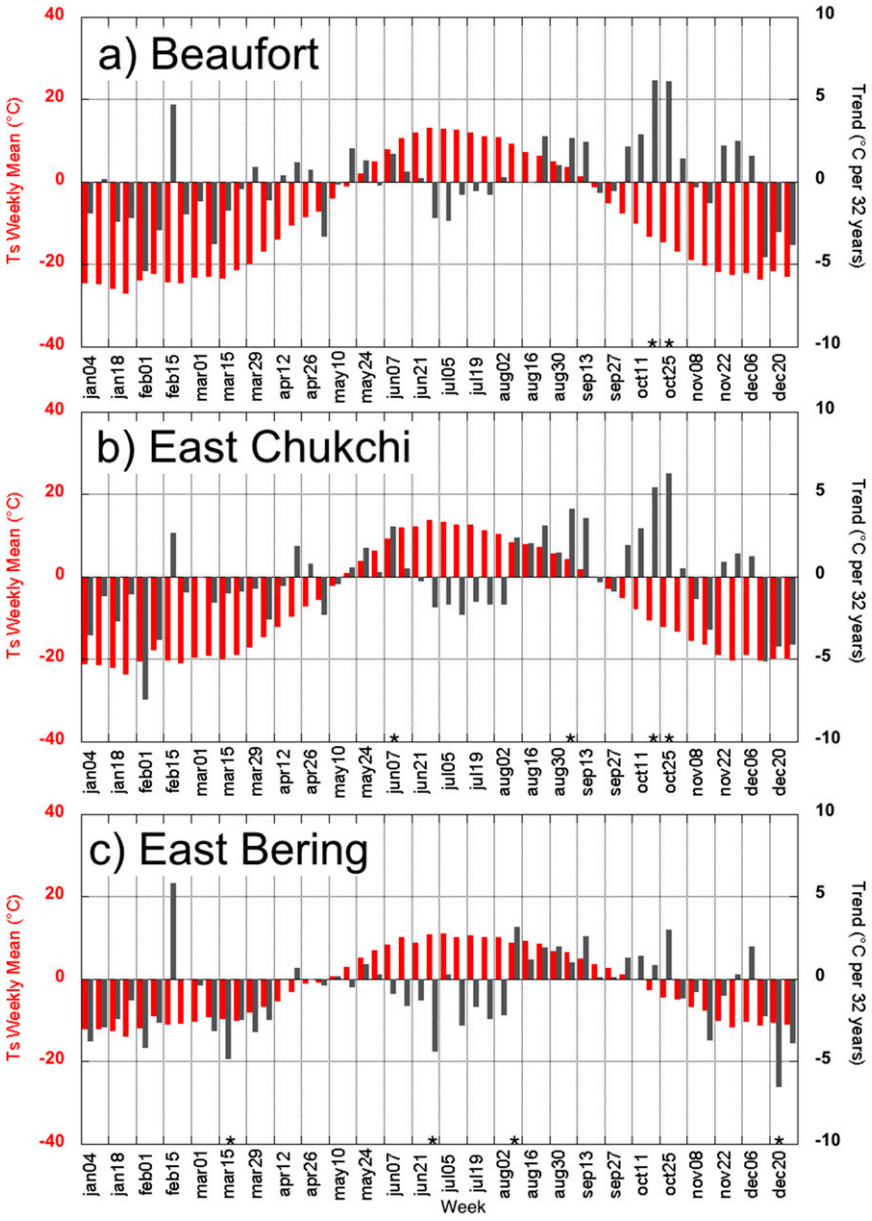

Figure 4. Weekly surface temperature Ts climatology (red) and trend magnitude change 1982–2013 (dark gray) for the (a) Beaufort, (b) east Chukchi, and (c) east Bering tundra regions. Weekly periods with trends significant at the 95% or greater level are marked with an asterisk on the *x* axis.

available for plant root growth, soil moisture, nutrient availability, and soil temperatures.

When SWE is evaluated weekly (Figure 6), several features are apparent: Climatologically, the east Chukchi has the highest mean SWE of the three regions, while the east Bering tends to have the longest snow-free season marked by the earliest melt of the regions. All three regions display positive trends of SWE in the

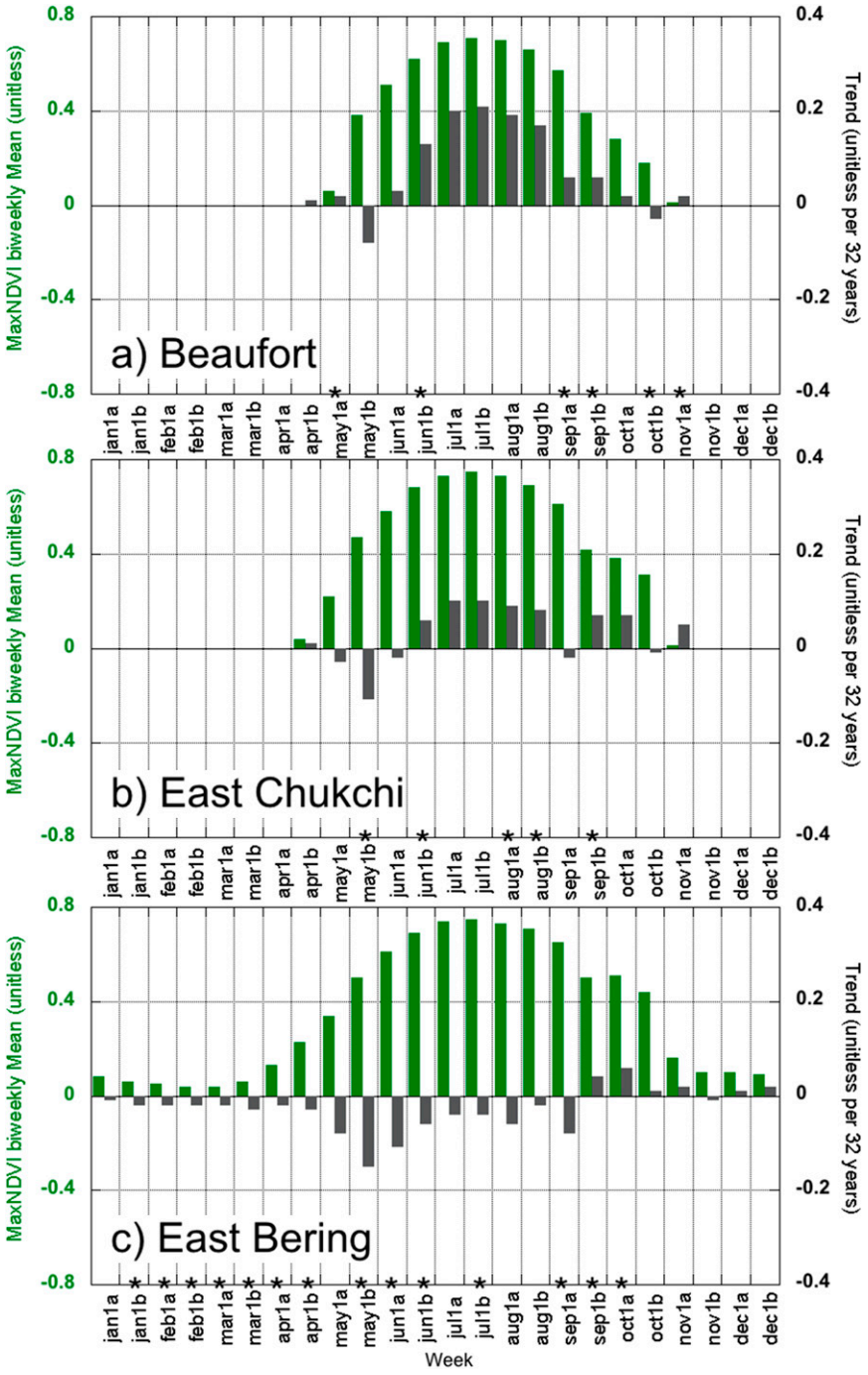

Figure 5. Biweekly NDVI climatology (green) and trend magnitude change 1982–2013 (dark gray) for the (a) Beaufort, (b) east Chukchi, and (c) east Bering tundra regions. Biweekly periods with trends significant at the 95% or greater level and a nonzero climatology are marked with an asterisk on the *x* axis.

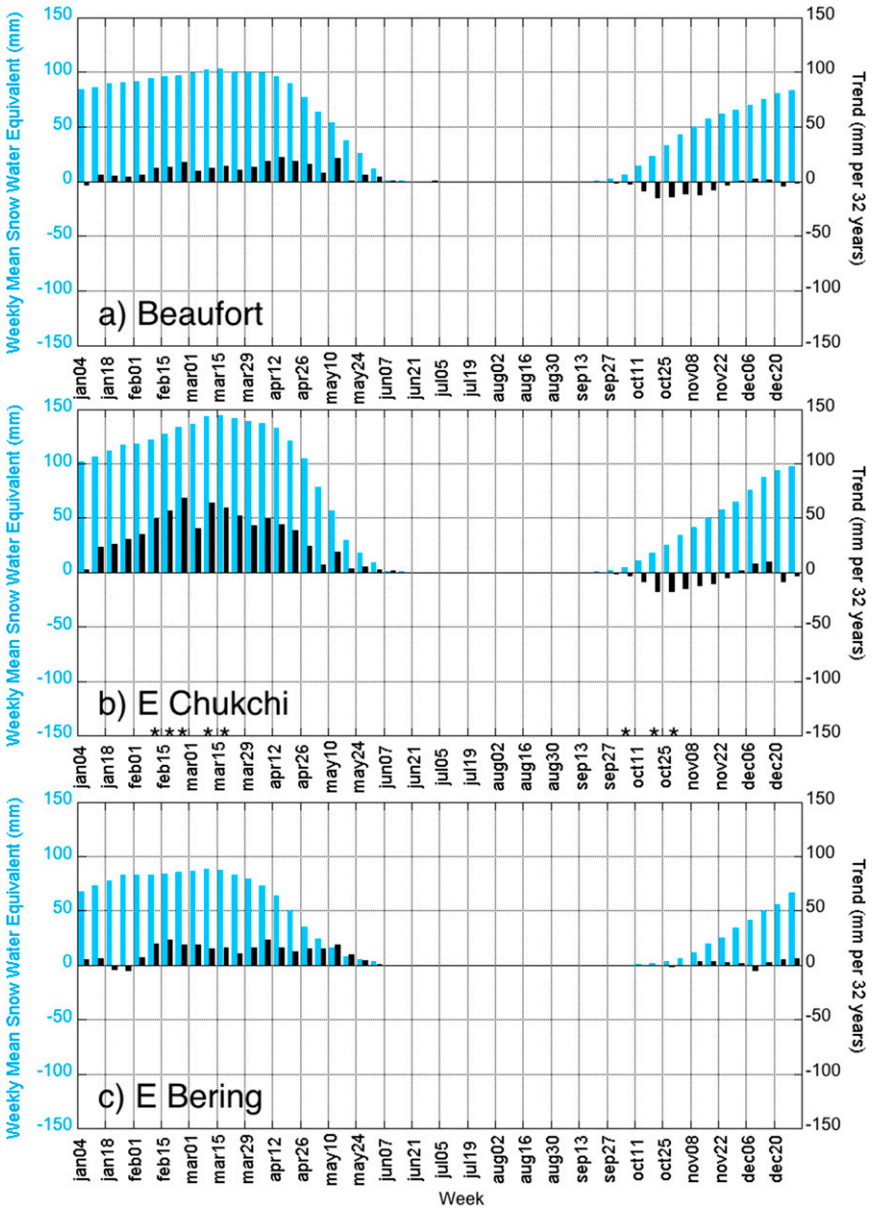

Figure 6. Weekly SWE climatology (blue) and trend magnitude change 1982–2013 (dark gray) for the (a) Beaufort, (b) east Chukchi, and (c) east Bering tundra regions. Weekly periods with trends significant at the 95% or greater level are marked with an asterisk on the *x* axis.

cold season, especially January–May. Only the east Bering has weak negative trends in midwinter SWE. The Beaufort and east Chukchi have trends toward reduced SWE in October–November, again corresponding to the enhanced temperatures and reduced sea ice occurring in the fall in these regions. This trend is consistent with warmer temperatures and late-season NDVI increases in these regions (see Figures 5a,b).

While the SWE data from GlobSnow have limited availability in late spring during the melt season, the trends toward increased spring SWE indicate a possible later melt date in the three tundra regions. Later melt is consistent with the declines in NDVI in the early growing season discussed in the previous section as more snow delays the onset of greenup. Enhanced winter snow depth and SWE in Arctic Alaska have also been noted in previous studies (Liston and Hiemstra 2011; Muskett 2012; Urban et al. 2014). Increased winter snow depth is also consistent with the hypothesis that increased snowfall in northern Alaska results from sea ice decline shown in climate modeling studies (Higgins and Cassano 2012; Liu et al. 2012a). Observational snow trends are not well synthesized across scales for Alaska, but several recent studies support the analysis presented here. Cherry et al. (2014) documented increased snow during spring at the Toolik Lake Research Station. Borehole temperature monitoring and snow depth records on the Alaska's North Slope that are maintained by the USGS on the National Petroleum Reserve (Urban and Clow 2014; Clow 2014) also found increases in snow depth and active layer warming at Fish Creek in winter and spring. The various observed snow increases are consistent with the recent declines in spring greening, though further analysis beyond the scope of this study is required to understand the extent of this variability.

3.3. Role of the large-scale atmospheric circulation in midsummer cooling trends

The second new pattern to emerge from the seasonality analysis is the decreasing temperature trends during the middle of the growing season in all three of the Alaskan tundra regions. This section explores processes that may explain the recent summer cooling. Variations in surface temperatures are likely linked to atmospheric processes at local and large scales. This component of the study focuses on the Beaufort and east Chukchi tundra regions and investigates cloud cover variations, circulation changes, and possible local climate mechanisms that could explain the recent midsummer cooling. East Bering will be discussed as well where relevant information is available.

3.3.1. Cloud cover changes

Cloud cover during the Arctic summer can quickly change surface air temperature, and increased cloudiness could account for the recent decrease in midsummer temperatures. When the seasonality of observed station cloudiness at Barrow (Beaufort and east Chukchi regions), Kotzebue (east Chukchi), and Bethel (east Bering) are evaluated (Figure 7; see locations in Figure 1a), several features stand out. All three stations display a climatological maximum in cloudiness during the summer season with a minimum in the winter, and the trends are highly variable throughout the year. Barrow (Figure 7a) has the largest positive trends in cloudiness in fall and early winter, likely linked with sea ice declines in the adjacent seas (Figures 2a,b). All three stations display positive trends throughout much of the summer. While a single station is not enough to support large-scale changes in cloudiness, several other pieces of evidence are consistent with the idea of an increase in summer cloudiness. Bhatt et al. (2013; see Figure 7) showed that Arctic terrestrial sea level pressure has been generally lower in the 1999–2011 period

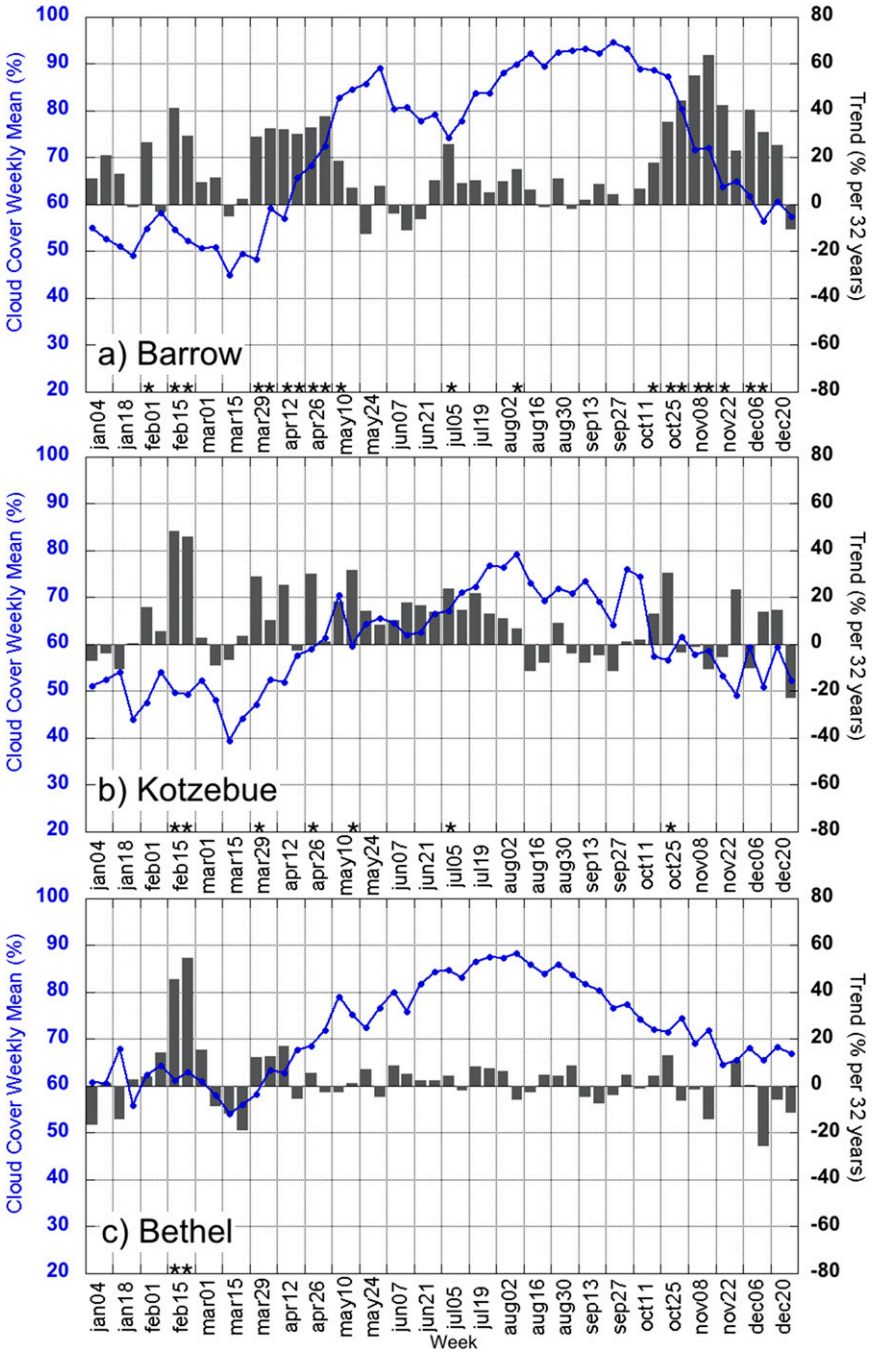

Figure 7. Weekly climatology of station cloudiness percent (blue lines) and trend magnitude change 1982–2013 (gray bars) at (a) Barrow, (b) Kotzebue, and (c) Bethel. Weekly periods with trends significant at the 95% or greater level are marked with an asterisk on the *x* axis.

compared to 1982–98 period, suggesting but not guaranteeing a higher possibility of cloudier conditions. In addition, a quantitative analysis by Liu et al. (2012b) found that from 2000 to 2010 MODIS cloud cover increased over the Arctic Ocean by approximately 0.4% for every 1% in sea ice decline. The correlation between the Beaufort and east Chukchi regional surface temperatures and the Barrow station cloudiness (Table 1) indicates that this station is a reasonable proxy for regional cloud cover as many of the correlations are statistically significant. There are periods of the year when the correlations between station cloudiness and regional temperatures are quite small, but the signs of the correlations are still consistent. Table 1 indicates that enhanced cloudiness in summer (winter) results in cooler (warmer) regional surface temperatures. The negative relationship in summer, coupled with the increases in cloudiness observed at the Barrow station suggest that cloudiness may be a key mechanism in driving the declines in surface temperature over the Beaufort and east Chukchi tundra regions in midsummer (see Figures 4a,b). This conclusion also seems to extend to the east Bering region, although the trends in cloudiness are much weaker there. A complicating factor here is that AVHRR temperatures are derived from clear-sky observations; therefore, the impact of cloudiness on temperatures in these data is not well defined, although the temperature response to cloudiness is physically consistent. However, limited observational temperature data are available in northern Alaska at the 30-yr climate scale, making the use of the relatively long, temporally and spatially consistent record of AVHRR advantageous. A detailed study of various historical gridded cloud products, including different types and elevation of clouds, is necessary to delve into the geographic patterns of cloudiness and more subtle changes in surface temperature.

3.3.2. Circulation changes

Circulation changes along coastal Alaska may also impact temperatures over land in northern Alaska and provide another possible explanation of the midsummer cooling. The Beaufort high is a major climatological feature over the Beaufort Sea (Overland 2009; Serreze and Barrett 2011) and typically extends over northern Alaska in June–August (Figure 8a). The Beaufort high may be a driver of change in cloud cover in northern Alaska. Previous studies have shown that the Beaufort high has strengthened during the summer in recent decades (Serreze and Barrett 2011; Moore 2012). The SLP trends over 1982–2013 show an increase or a strengthening of the Beaufort high over the Arctic Ocean while weakening over northern Alaska in June–August (Figure 8a). However, there is seasonality in the trends and position of the high pressure center (Figures 8b–d). June (Figure 8b) stands out as the month with SLP increasing along the Beaufort coast, while July (Figure 8c) has significant declines in SLP over all of northern and western Alaska. The SLP trends in August (Figure 8d) are more intermediate to those of June and July. When weekly SLP was extracted from a box including the Beaufort Sea (70° to 80°N latitude and 120°E to 180° longitude), the seasonality shows mixed trends throughout the year (Figure 9) that match the monthly findings of Figure 8 with increasing SLP in June, decreasing SLP in July, and mixed trends in August. Correlating the Barrow station cloudiness with the weekly SLP

Table 1. Weekly correlation of Beaufort and east Chukchi Ts and Beaufort high area average sea level pressure with Barrow station cloudiness. Correlations significant at the 90% (95%) level are shown in italic (bold).

	Correlation vs Barrow cloudiness		
Week	Beaufort Ts	E Chukchi Ts	BH box SLP
4 Jan	**0.54**	**0.48**	*−0.31*
11 Jan	**0.37**	**0.38**	−0.13
18 Jan	**0.50**	**0.35**	−0.29
25 Jan	**0.48**	0.28	*−0.30*
1 Feb	**0.44**	**0.39**	0.03
8 Feb	*0.35*	**0.36**	0.04
15 Feb	**0.60**	**0.57**	**−0.40**
22 Feb	0.18	0.05	**−0.37**
1 Mar	**0.48**	**0.40**	−0.11
8 Mar	**0.44**	0.17	−0.24
15 Mar	**0.47**	0.25	*−0.30*
22 Mar	**0.55**	0.29	**−0.38**
29 Mar	**0.37**	0.20	**−0.37**
5 Apr	**0.60**	**0.49**	−0.17
12 Apr	0.19	0.12	**−0.52**
19 Apr	**0.56**	**0.47**	−0.13
26 Apr	0.24	0.12	0.10
3 May	0.27	0.08	**−0.36**
10 May	*0.31*	0.15	**−0.46**
17 May	−0.15	−0.21	−0.06
24 May	**−0.53**	**−0.59**	−0.19
31 May	−0.26	−0.16	−0.11
7 Jun	−0.19	**−0.40**	−0.27
14 Jun	**−0.42**	−0.29	0.05
21 Jun	−0.20	**−0.46**	−0.21
28 Jun	−0.15	**−0.37**	0.00
5 Jul	*−0.35*	**−0.50**	**−0.56**
12 Jul	**−0.35**	**−0.43**	**−0.54**
19 Jul	*−0.32*	**−0.40**	**−0.40**
26 Jul	**−0.35**	**−0.47**	−0.28
2 Aug	−0.21	**−0.42**	−0.17
9 Aug	**−0.45**	−0.24	−0.21
16 Aug	−0.24	−0.02	−0.11
23 Aug	*−0.32*	−0.25	−0.30
30 Aug	**−0.36**	**−0.42**	−0.26
6 Sep	0.01	−0.07	−0.11
13 Sep	−0.03	−0.18	0.20
20 Sep	**−0.56**	**−0.50**	0.03
27 Sep	−0.30	−0.25	0.05
4 Oct	−0.08	−0.04	0.21
11 Oct	−0.14	0.04	0.24
18 Oct	0.02	−0.05	0.12
25 Oct	−0.02	−0.06	−0.21
1 Nov	0.23	0.29	−0.23
8 Nov	**0.58**	**0.46**	−0.20
15 Nov	*0.33*	0.29	−0.27
22 Nov	**0.37**	0.15	**−0.44**
29 Nov	*0.32*	0.14	*−0.31*
6 Dec	**0.51**	*0.33*	−0.13
13 Dec	0.16	−0.11	**−0.36**
20 Dec	**0.37**	0.21	0.01
27 Dec	0.19	0.11	**−0.37**

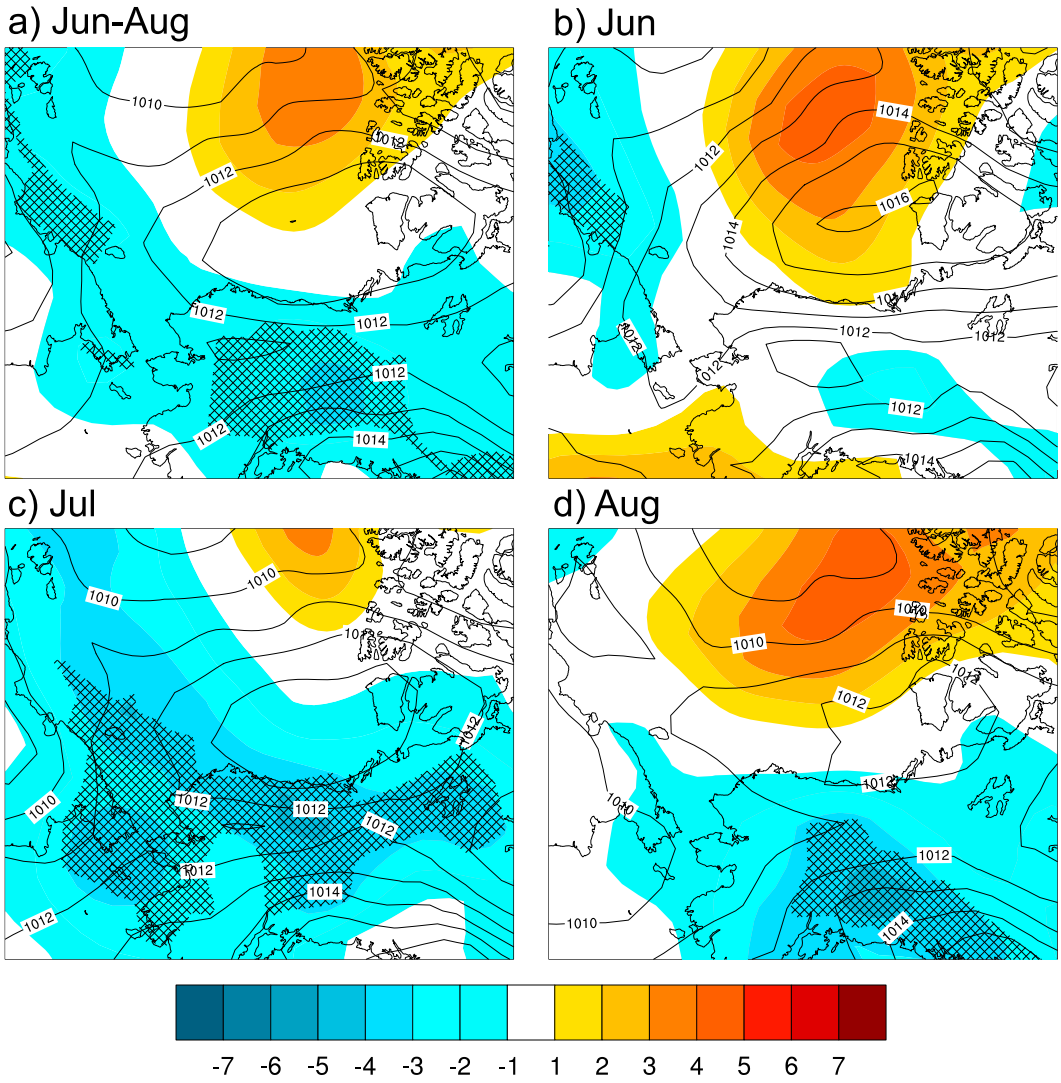

Figure 8. Mean sea level pressure climatology (contours) and trend magnitude change 1982–2013 (shaded) for (a) June–August, (b) June, (c) July, and (d) August. Units are hPa for the climatology and hPa $(32\,\mathrm{yr})^{-1}$ for the trends. Trends significant at the 95% or greater level are shown by cross hatching.

(Table 1) indicates that higher SLP associated with the Beaufort high results in increased subsidence and reduced cloudiness at the Barrow station. This finding supports a link between the strength of the Beaufort high and surface temperatures that subsequently impact NDVI. However, many of the correlations between SLP and the Barrow station cloud observation are fairly weak outside of July, pointing to a complex mechanism. One possible complication is that a strengthened (weakened) Beaufort high could also enhance (decrease) northeasterly winds. Enhanced northeasterly winds would advect moisture and clouds from the Arctic Ocean inland over the region and cause cooling. Given the

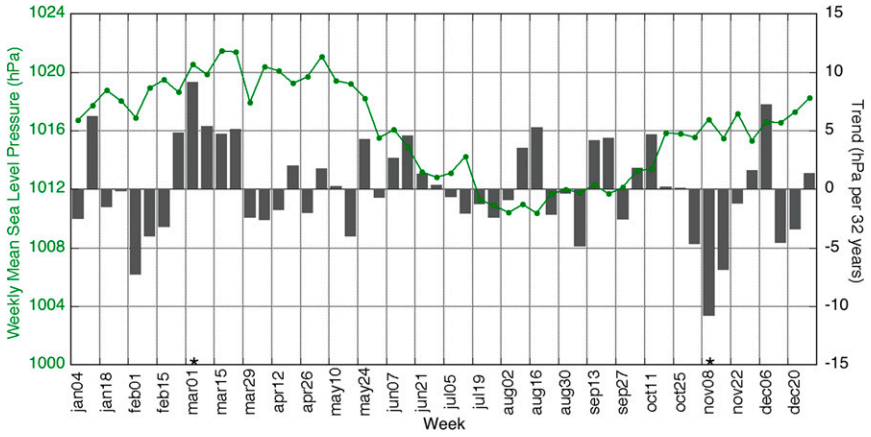

Figure 9. Weekly SLP climatology (green line) and trend magnitude change 1982–2013 (gray bars) based on an area average of the Beaufort high region defined as 70° to 80°N latitude and 120°E to 180° longitude. Weekly periods with trends significant at the 95% or greater level are marked with an asterisk on the *x* axis.

signs and significance of the correlations coupled with significant declining trends in SLP over land in July, it appears that the reduced subsidence associated with a weakened Beaufort high is driving midsummer cooling in the northern Alaska tundra regions by enhanced cloudiness. However, few high spatial resolution cloud observations exist at the climate time scale to fully diagnose the other unknowns in this mechanism. Using modeling or long-term gridded cloud cover data as they become available would be prudent in future studies.

The east Bering is close to the North Pacific Ocean, that is, far from the effect of the Beaufort high. Thus, the east Bering region is influenced by a different atmospheric circulation regime than the northern Beaufort and east Chukchi regions. The declines in NDVI in the east Bering region occur with later snowmelt and enhanced late winter/spring sea ice in the adjacent Bering Sea. The west Pacific pattern (WP) is a mode of atmospheric variability in the Pacific that influences the strength of a trough or low pressure in the atmospheric circulation centered over the Bering Sea (Wallace and Gutzler 1981). Increased sea ice in the eastern Bering Sea region has been linked with the positive phase of the WP (Matthewman and Magnusdottir 2011). The positive phase of the WP represents a strengthening of the low pressure over the Bering Sea region. Low pressure, while advecting moisture from the Pacific, also brings clouds that reduce temperatures and increase precipitation in the spring in Alaska (Bieniek et al. 2011) and advects sea ice from the north. More frequent positive phases of the WP since the 1980s (Linkin and Nigam 2008) may be driving the increases in spring sea ice and the trend to later snowmelt in the east Bering region. The trend of delayed snowmelt due to late-season snowfall in the east Bering region is consistent with increased cloud cover, precipitation, and reduced temperatures brought about by low pressure over the Bering Sea enhanced by the WP.

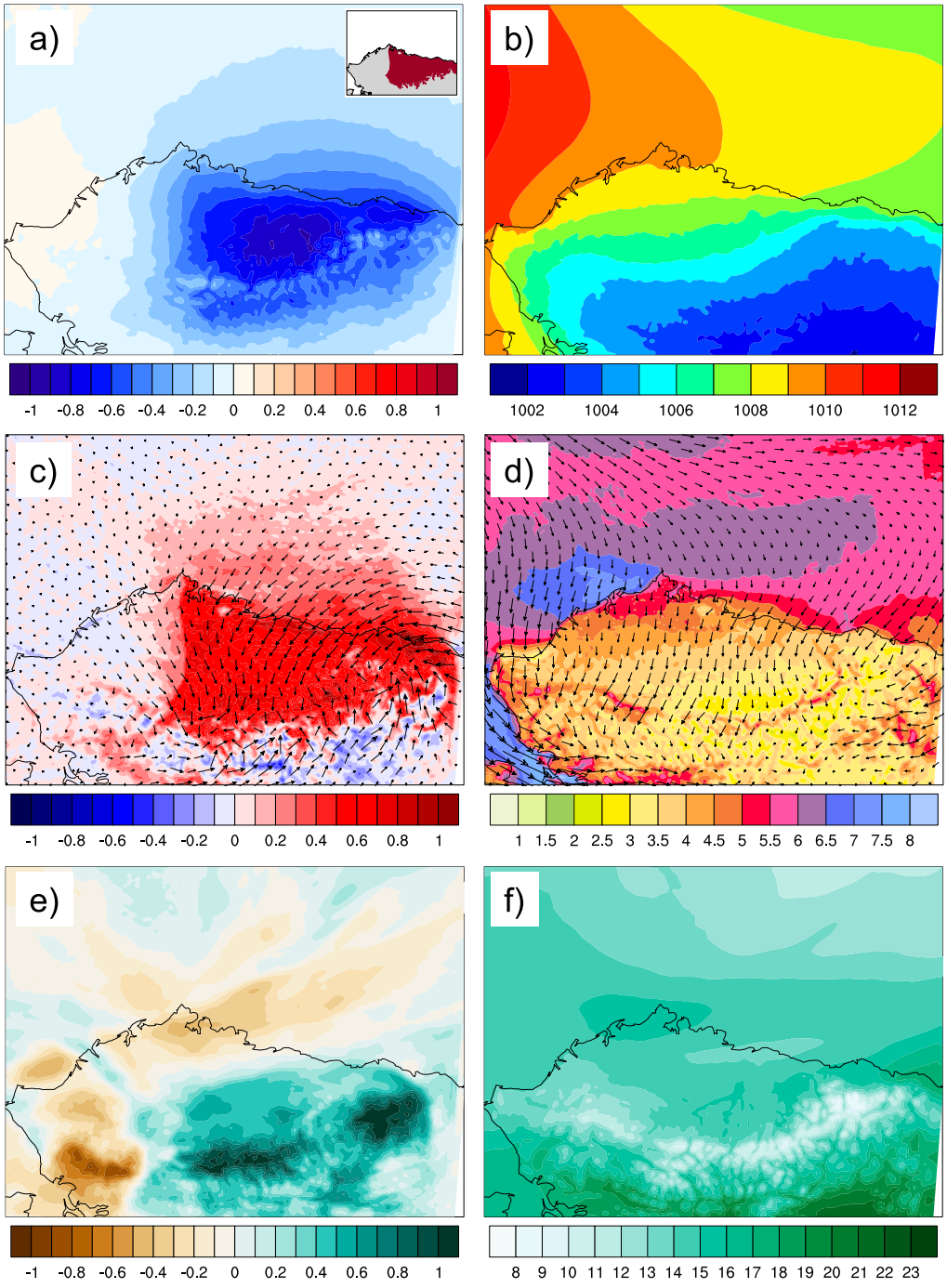

Figure 10. Warm anomaly minus reference WRF Model simulation average and reference simulation average for July for (a),(b) SLP, (c),(d) 10-m wind, and (e),(f) column precipitable water. The units are hPa, m s^{-1}, and mm for SLP, 10-m wind, and precipitable water, respectively. The anomalous wind vectors are displayed in (c). The area where the +3°C anomaly was imposed in the WRF Model is shown in the inset map in (a).

3.4. Role of the local atmospheric circulation in midsummer cooling trends

Local atmospheric circulation/feedback processes are another possible source for the midsummer cooling trends observed in the coastal tundra regions. The local summer climate of the Beaufort and east Chukchi tundra regions is influenced by the position of the Arctic frontal boundary, which marks the boundary between the cold air mass of the Arctic Ocean and the warmer air mass of Interior Alaska (Conover 1960). These regions consistently experience sea breezes in summer (Moritz 1977; Walsh 1977; Kozo 1979). Sea breezes result from the land–sea temperature contrast. The air over the land, warmed by the solar heating of the surface, rises and the relatively cooler air over the ocean moves in underneath resulting in wind blowing from the water toward the land. These sea breezes have a great influence on the spatial patterns of temperatures during the warm season in this region (Haugen and Brown 1980; Kozo 1982). They also influence the vegetation patterns inland (Walker 1985), the distribution of road dust downwind of the roads in summer (Benson et al. 1975; Everett 1980), and even the mosquito and caribou movements and distributions (White et al. 1975). Temperatures farther inland near the Brooks Range tend to be more influenced by the amount of cloudiness than the sea breeze since the sea breeze usually does not extend so far inland from the coast (Zhang et al. 1996).

Increasing land surface temperatures in early summer could be responsible for enhancing the sea-breeze circulation and influencing cloud cover. Warming has been noted as a possible feedback response to increased shrubs, which reduce albedo in the Arctic (Chapin et al. 2005). The large-scale circulation may also give rise to warming as the enhanced Beaufort high may lead to decreased cloudiness. However, an enhanced Beaufort high may lead to more favorable conditions for the cooling sea-breeze circulation to form as they form more easily under the weak flow conditions of strong high pressure. The observed declines in sea ice and increases of ocean heat content may also affect the changes of the local circulation in northern Alaska.

One hypothesis is that a negative feedback may result from the enhanced circulation due to the land surface warming, giving rise to cloudiness and convection over the land where convergence in the sea-breeze circulation occurs and thus cooling land surface temperatures in addition to the cooling effect of the enhanced onshore winds themselves. Because of the lack of station observational data at the spatial resolution needed to best evaluate the sea-breeze circulation and other local atmospheric changes, the WRF Model was utilized to examine the local atmospheric response to warming or cooling the land surface by 3°C over the Beaufort region (the boundaries of the Beaufort region are shown in Figure 1a). The findings of the June and July portions were similar; therefore, those for July (Figure 10) are shown for simplicity. When positive temperature anomalies were applied to the land surface in the WRF Model, the atmosphere responded by reducing sea level pressure by more than 0.5 hPa over the entire Beaufort tundra region (Figure 10a) relative to the reference simulation (Figure 10b). A broad comparison may also be made between the reduced SLP shown in the model sensitivity study (Figures 10a) and the observed significant decline in SLP over the Beaufort and east Chukchi regions in July (Figure 8c). The

increased temperatures over land also resulted in enhanced onshore 10-m winds across the Beaufort Sea coast (Figure 10c) relative to the reference simulation (Figure 10d), likely due to the enhanced land–sea/ice temperature contrast enhancing the sea-breeze circulation. The enhanced northerly onshore winds may also have had the effect of reducing the precipitable water in the atmospheric column along the coast (Figure 10e) relative to the reference simulation (Figure 10f). Enhanced convergence of the air against the Brooks Range in the southern portion of the domain due to the increased northerly winds in Figure 10c further lead to increased precipitable water inland over the Beaufort region. Increased precipitable water indicates that more moisture is available in the atmospheric column to form clouds and precipitation.

The results of this simple model sensitivity experiment indicate that when the surface has warmed sufficiently (e.g., from increased vegetation productivity), the sea-breeze circulation is strengthened and could act to reduce temperatures over the land surface as a negative feedback. In addition, precipitable water is enhanced inland from the coast in response to the surface warming, which can lead to increased cloudiness and precipitation also causing a negative feedback that would reduce temperatures over the land surface. The enhanced sea-breeze circulation response indicated by the WRF Model is consistent with the trend to increased wind speeds observed along the coast in reanalysis in recent decades (Stegall and Zhang 2012). In addition, the reduced SLP response to the surface temperature anomaly in the WRF Model is consistent with the reduction in SLP that has been observed over northern Alaska in July, associated with a weakened Beaufort high. The results are also consistent with the observed increase in cloudiness; however, an improved gridded cloudiness dataset with coverage of the Beaufort region would be necessary to investigate if cloudiness is increasing inland to be fully consistent with the feedback mechanism presented here.

These results demonstrate that it is possible that surface warming due to enhanced vegetation following a mechanism similar to Chapin et al. (2005) or even other large-scale causes such as reduced cloudiness under enhanced high pressure could have a local cooling response through enhanced sea-breeze circulations and cloudiness/precipitation in a region like the Beaufort. The feedback response also has further impacts on the larger-scale SLP. One caveat is that it is uncertain if the tundra vegetation has increased enough to result in extensive surface temperature changes especially of the magnitude used in this highly idealized model experiment. Additional model experiments are needed to better link changes in the sea-breeze circulation to midsummer cooling. Such simulations should better account for sea ice and increased open water, as this simulation had extensive sea ice throughout, and be further expanded to examine the role of snowmelt timing in the feedbacks. Also, the anomaly was fixed in this WRF Model experiment; therefore, land surface temperatures could not respond to enhanced cloudiness or cooling due to the sea breeze. Further experiments allowing the land surface temperatures and vegetation to respond to changes will also be needed to better evaluate potential feedbacks. Additional atmospheric and vegetation observational data will be needed in the future to assess if similar local feedback mechanisms are operating in the east Bering tundra region and driving or enhancing the midsummer cooling there.

4. Synthesis

Climatic changes impacting vegetation and NDVI have been documented in the coastal regions of Alaska for 1982–2013. The trends display a clear seasonality that is due to the interplay of different mechanisms at both local and larger scales. The three coastal tundra regions of Alaska also have different linkages with the local- and large-scale climate and impacts due to their vast geographic areas that span from the Pacific to the Arctic Oceans. As a result, the trends and the mechanisms are summarized separately for Alaska's three coastal tundra regions.

The Beaufort tundra region has experienced the largest amount of greening of the three Alaskan tundra regions. The adjacent Beaufort Sea has seen enhanced ocean heat content in summer and declining sea ice throughout the summer but mostly in spring and fall. The Beaufort region has experienced increased snow in the spring and later snowmelt; however, the onset of snow has been occurring later in fall. Enhanced spring snow cover is likely driving the early season decline in NDVI through a delayed onset of the growing season. Temperatures had variable trends throughout the year with cooling in midsummer. The midsummer decline is linked to increased cloudiness in the region in summer as observed at Barrow. The cloudiness and temperature are also linked to subseasonal variability in the Beaufort high. While the Beaufort high has strengthened in summer, there has been a decline in strength in midsummer that corresponds to the midsummer cooling trend. An idealized model experiment showed that this cooling could also be due to the impact of changes in terrestrial surface temperatures in the region impacting the sea-breeze circulation, which also relates to the strength and/or position of the Beaufort high as well as cloudiness. This result indicates that a negative feedback from warming will result; warming of the land enhances the sea breeze, which then brings in cooler air from the Arctic Ocean and thus cooling the land. The second component of the negative feedback is that convergence from the sea breeze may lead to enhanced cloudiness, resulting in cooling farther inland. Another factor to be considered with enhanced easterly winds is the potential for increased upwelling of relatively colder deep waters along the Beaufort Sea coast that could reduce sea surface temperatures and ultimately impact the sea-breeze circulation. Based on our findings, ocean heat content has increased over the period of record over the Beaufort Sea region defined by this study. Studies have shown that there has mainly been a warming in sea surface temperatures across the entire region (including right along the coast), indicating that any cooling due to upwelling is playing a small role compared to the broader warming there (Steele et al. 2008). It is possible that the warming could be due to the movement of warmer water along the coast, and sea ice may also be playing a large role too; however, more analysis will be needed to better understand the mechanisms that are driving the changes in ocean heat content. Specific questions that remain for the Beaufort tundra region are as follows: What is the role of sea ice/sea surface temperatures in the sea-breeze circulation? What is the role of convection? Do changes in vegetation impact the atmosphere?

The east Chukchi coastal tundra region is adjacent to the Beaufort region and has therefore experienced similar seasonality in trends and has similar linkages to climate drivers. While there are similarities to the Beaufort region, the trends tend to be weaker. Sea ice has declined throughout the summer with the greatest declines in spring and fall. Ocean heat content has increased; however, the maximum

trends are nearly half of those of the Beaufort. NDVI has increased throughout much of the season, and there is an early season decline. The east Chukchi region exhibits a similar seasonality of temperature variability and trends as the Beaufort region, displaying midsummer cooling with warming in early and late summer. SWE has increased in spring with a later melt date likely contributing to the early season decline in NDVI. Like the Beaufort region, lower summer temperatures are linked to the variability of the Barrow cloudiness observations and the strength of the Beaufort high. Because of its location adjacent to the Beaufort sea-breeze zone, it is hypothesized that a similar sea breeze/cloudiness land surface feedback mechanism is at play. Similar questions remain to those of the Beaufort region with some additional ones: Because the east Chukchi zone is located along the Bering Sea, what is the role of the Pacific climate?

The east Bering coastal tundra region has experienced distinctive changes driven by different climate drivers than the northerly Beaufort and east Chukchi regions. Unlike the Beaufort and east Chukchi, NDVI has declined throughout the season. The greatest declines have been in the early season. Sea ice has increased in spring, and the Bering Sea is normally ice free in summer. Ocean heat content has declined throughout the spring and summer. However, similar variability in the seasonality of temperature occurs as in the other tundra regions. Spring SWE has increased with later melt, likely consistent with the early season declines in NDVI. An additional linkage has been previously identified showing that the recently enhanced west Pacific pattern has been advecting colder air and sea ice down into the Bering Sea, resulting in the delayed onset of the growing season. It is postulated that this delay is playing a role in the overall seasonal NDVI declines. Much remains uncertain for the east Bering: Have physiological changes occurred to the plants that explain the NDVI decline? Are there other local atmospheric drivers at work like the sea breeze in the Beaufort? Are changes in the winter snowpack (e.g., later onset, time of major snowfall, SWE, and snow depth) and its impacts (e.g., soil insulation and active layer depth) playing a role in the NDVI change? Addressing this last question has potential merit as local expert knowledge from Native Alaskan elders in the east Bering region has suggested that changes in the characteristics of snow cover have occurred (Fienup-Riordan and Rearden 2012). Native Alaskan elders have indicated that the timing of the berry harvest is occurring earlier within their memory and that the harvest is now less plentiful and appears tied to the winter snowfall (Fienup-Riordan and Rearden 2012). Future analysis is recommended to evaluate these linkages.

The east Bering is more of a maritime tundra region than the other Alaskan regions and may more closely follow processes in the Norwegian maritime tundra, where Bjerke et al. (2014) reported vegetation declines in evergreen vegetation (*Empetrum nigrum* and *Juniperus communis*) due to winter warming events that reduced the protective snow cover leading to plant damage. It is likely that numerous factors are responsible for vegetation declines in the east Bering region.

5. Conclusions

In Alaska, both the large- and local-scale climate play a role in the seasonality of NDVI and temperature variability in Arctic coastal tundra regions. Enhanced spring snow cover is likely driving a decline in early season NDVI in all three

tundra regions. The delayed onset of the growing season appears to have an especially pronounced impact in the east Bering and may be driving the overall seasonal decline in NDVI there. Midsummer temperatures have declined in all three tundra regions of Alaska, just as has been observed throughout the pan-Arctic (Bhatt et al. 2013). Our analysis indicates that a declining Beaufort high over northern Alaska in midsummer is driving enhanced cloudiness and lower temperatures in the Beaufort and east Chukchi regions. In addition, local feedbacks due to the sea-breeze circulation and cloudiness may play a role in the declining temperatures as well. Additional analysis and modeling may shed light on the large-scale linkages and local feedbacks that are driving the cooling. However, they require a detailed analysis of the spatial changes in NDVI to impose realistic vegetation changes in future regional model sensitivity studies to fully diagnose those feedbacks. Such data analysis and hypothesis testing by modeling could provide insight into the interaction of vegetation and local atmospheric processes through evapotranspiration and/or albedo. Since snow is an essential variable for understanding mechanisms of vegetation change in the Arctic, efforts to advance our observational snow datasets should also be a priority.

Acknowledgments. The authors thank Jim Overland, John Walsh, Matthew Sturm, Torre Jorgenson, Xiangdong Zhang, Debasish Pai Mazumder, Ann Fienup-Riordan, Alice Reardon, Mark John, the members of the Calista Elders Council, and the two anonymous reviewers for their fruitful discussions that helped to improve this study. This study was supported by funds from NSF Grants ARC-051180, ARC-0902175, ARC-0902042, and ARC-0901987, NASA Grants NNG6NEA00A and NNX13AE29G, the USGS Alaska Climate Science Center, and the University of Alaska Fairbanks Office of the Vice Chancellor for Research.

References

Beck, P. S. A., and Coauthors, 2011: Changes in forest productivity across Alaska consistent with biome shift. *Ecol. Lett.*, **14**, 373–379, doi:10.1111/j.1461-0248.2011.01598.x.

Bekryaev, R. V., I. V. Polyakov, and V. A. Alexeev, 2010: Role of polar amplification in long-term surface air temperature variations and modern Arctic warming. *J. Climate*, **23**, 3888–3906, doi:10.1175/2010JCLI3297.1.

Benson, C., B. Holmgren, R. Timmer, G. Weller, and S. Parrish, 1975: Observations on the seasonal snow cover and radiation climate at Prudhoe Bay, Alaska during 1972. *Ecological Investigations of the Tundra Biome at Prudhoe Bay, Alaska*, J. Brown, Ed., Biological Papers of the University of Alaska, Special Rep. 2, University of Alaska, 12–50.

Berner, J., and Coauthors, 2005: *Arctic Climate Impact Assessment.* Cambridge University Press, 1046 pp.

Bhatt, U. S., M. A. Alexander, C. Deser, J. E. Walsh, J. S. Miller, M. S. Timlin, J. Scott, and R. A. Tomas, 2008: The atmospheric response to realistic reduced summer Arctic sea ice anomalies. *Arctic Sea Ice Decline: Observations, Projections, Mechanisms, and Implications*, *Geophys. Monogr.*, Vol. 180, Amer. Geophys. Union, 91–110.

——, and Coauthors, 2010: Circumpolar Arctic tundra vegetation change is linked to sea ice decline. *Earth Interact.*, **14**, doi:10.1175/2010EI315.1.

——, and Coauthors, 2013: Recent declines in warming and vegetation greening trends over pan-Arctic tundra. *Remote Sens.*, **5**, 4229–4254, doi:10.3390/rs5094229.

——, and Coauthors, 2014: Implications of Arctic sea ice decline for the Earth system. *Annu. Rev. Environ. Resour.*, **39**, 57–89, doi:10.1146/annurev-environ-122012-094357.

Bieniek, P. A., U. S. Bhatt, L. A. Rundquist, S. D. Lindsey, and X. D. Zhang, 2011: Large-scale climate controls of Interior Alaska River ice breakup. *J. Climate*, **24**, 286–297, doi:10.1175/2010JCLI3809.1.

——, and Coauthors, 2012: Climate divisions for Alaska based on objective methods. *J. Appl. Meteor. Climatol.*, **51**, 1276–1289, doi:10.1175/JAMC-D-11-0168.1.

——, J. E. Walsh, R. L. Thoman, and U. S. Bhatt, 2014: Using climate divisions to analyze variations and trends in Alaska temperature and precipitation. *J. Climate*, **27**, 2800–2818, doi:10.1175/JCLI-D-13-00342.1.

Bjerke, J. W., S. R. Karlsen, K. A. Høgda, E. Malnes, J. U. Jepsen, S. Lovibond, D. Vikhamar-Schuler, and H. Tømmervik, 2014: Record-low primary productivity and high plant damage in the Nordic Arctic region in 2012 caused by multiple weather events and pest outbreaks. *Environ. Res. Lett.*, **9**, 084006, doi:10.1088/1748-9326/9/8/084006.

Cantlon J. E., 1961: Plant cover in relation to macro-, meso-, and micro-relief. Office of Naval Research Final Rep., Grants ONR-208 and ONR-216, 128 pp.

Chapin, F. S., and Coauthors, 2005: Role of land-surface changes in Arctic summer warming. *Science*, **310**, 657–660, doi:10.1126/science.1117368.

Cherry, J. E., S. Déry, A. S. Jacobs, Y. Chen, and M. Stieglitz, 2014: Climate and hydrometeorology of the Toolik Lake region and Kuparuk River basin: Past, present and future. *Alaska's Changing Arctic*, J. Hobbie, Ed., Oxford University Press, 310 pp.

Chou, M.-D., and M. J. Suarez, 1994: An efficient thermal infrared radiation parameterization for use in general circulation models. NASA Tech. Memo. 104606, 85 pp.

Clow, G. D., 2014: Temperature data acquired from the DOI/GTN-P deep borehole array on the Arctic slope of Alaska, 1973–2013. *Earth Syst. Sci. Data*, **6**, 201–218, doi:10.5194/essd-6-201-2014.

Comiso, J. C., 2003: Warming trends in the Arctic from clear sky satellite observations. *J. Climate*, **16**, 3498–3510, doi:10.1175/1520-0442(2003)016<3498:WTITAF>2.0.CO;2.

——, and F. Nishio, 2008: Trends in the sea ice cover using enhanced and compatible AMSR-E, SSM/I, and SMMR data. *J. Geophys. Res.*, **113**, C02S07, doi:10.1029/2007JC004257.

Conover, J. H., 1960: Macro- and microclimatology of the Arctic slope of Alaska. U.S. Army Headquarters Quartermaster Research and Engineering Command Tech. Rep. EP-139, 65 pp.

Deering, D. W., 1978: Rangeland reflectance characteristics measured by aircraft and spacecraft sensors. Ph.D. dissertation, Texas A&M University, 338 pp.

Dutrieux, L. P., H. Bartholomeus, M. Herold, and J. Verbesselt, 2012: Relationships between declining summer sea ice, increasing temperatures and changing vegetation in the Siberian Arctic tundra from MODIS time series (2000–11). *Environ. Res. Lett.*, **7**, 044028, doi:10.1088/1748-9326/7/4/044028.

Epstein, H. E., and Coauthors, 2004: The nature of spatial transitions in the Arctic. *J. Biogeogr.*, **31**, 1917–1933, doi:10.1111/j.1365-2699.2004.01140.x.

——, M. K. Raynolds, D. A. Walker, U. S. Bhatt, C. J. Tucker, and J. E. Pinzon, 2012: Dynamics of aboveground phytomass of the circumpolar Arctic tundra during the past three decades. *Environ. Res. Lett.*, **7**, 015506, doi:10.1088/1748-9326/7/1/015506.

Everett, K. R., 1980: Distribution and properties of road dust along the northern portion of the Haul Road. U.S. Army Cold Regions Research and Engineering Laboratory CRREL Rep. 80-19, 101−128.

Fienup-Riordan, A., and A. Rearden, 2012: *Ellavut: Our Yup'ik World and Weather.* University of Washington Press, 354 pp.

Grell, G. A., and D. Dévényi, 2002: A generalized approach to parameterizing convection combining ensemble and data assimilation techniques. *Geophys. Res. Lett.*, **29**, doi:10.1029/2002GL015311.

Haugen, R. K., and J. Brown, 1980: Coastal-inland distributions of summer air temperature and precipitation in northern Alaska. *Arct. Alp. Res.*, **12**, 403–412, doi:10.2307/1550491.

Higgins, M. E., and J. J. Cassano, 2012: Northern Alaskan land surface response to reduced Arctic sea ice extent. *Climate Dyn.*, **38**, 2099–2113, doi:10.1007/s00382-011-1095-0.

Hong, S.-Y., and J.-O. J. Lim, 2006: The WRF single-moment 6-class microphysics scheme (WSM6). *J. Korean Meteor. Soc.*, **42**, 129–151.

Janjić, Z. I., 2002: Nonsingular implementation of the Mellor-Yamada level 2.5 scheme in the NCEP meso model. NCEP Office Note 456, 61 pp.

Jia, G. S. J., H. E. Epstein, and D. A. Walker, 2003: Greening of Arctic Alaska, 1981–2001. *Geophys. Res. Lett.*, **30**, 2067, doi:10.1029/2003GL018268.

Kalnay, E., and Coauthors, 1996: The NCEP/NCAR 40-Year Reanalysis Project. *Bull. Amer. Meteor. Soc.*, **77**, 437–471, doi:10.1175/1520-0477(1996)077<0437:TNYRP>2.0.CO;2.

Kozo, T. L., 1979: Evidence for sea breezes on the Alaskan Beaufort Sea coast. *Geophys. Res. Lett.*, **6**, 849–852, doi:10.1029/GL006i011p00849.

——, 1982: An observational study of sea breezes along the Alaskan Beaufort Sea coast: Part I. *J. Appl. Meteor.*, **21**, 891–905, doi:10.1175/1520-0450(1982)021<0891:AOSOSB>2.0.CO;2.

Lawrence, D. M., A. G. Slater, R. A. Tomas, M. M. Holland, and C. Deser, 2008: Accelerated Arctic land warming and permafrost degradation during rapid sea ice loss. *Geophys. Res. Lett.*, **35**, L11506, doi:10.1029/2008GL033985.

Linkin, M. E., and S. Nigam, 2008: The North Pacific Oscillation–west Pacific teleconnection pattern: Mature-phase structure and winter impacts. *J. Climate*, **21**, 1979–1997, doi:10.1175/2007JCLI2048.1.

Liston, G. E., and C. A. Hiemstra, 2011: The changing cryosphere: Pan-Arctic snow trends (1979–2009). *J. Climate*, **24**, 5691–5712, doi:10.1175/JCLI-D-11-00081.1.

Liu, J. P., J. A. Curry, H. J. Wang, M. R. Song, and R. M. Horton, 2012a: Impact of declining Arctic sea ice on winter snowfall. *Proc. Natl. Acad. Sci. USA*, **109**, 4074–4079, doi:10.1073/pnas.1114910109.

Liu, Y., J. R. Key, Z. Liu, X. Wang, and S. J. Vavrus, 2012b: A cloudier Arctic expected with diminishing sea ice. *Geophys. Res. Lett.*, **39**, L05705, doi:10.1029/2012GL051251.

Macias-Fauria, M., B. C. Forbes, P. Zetterberg, and T. Kumpula, 2012: Eurasian Arctic greening reveals teleconnections and the potential for structurally novel ecosystems. *Nat. Climate Change*, **2**, 613–618, doi:10.1038/nclimate1558.

Manabe, S., J. Ploshay, and N. C. Lau, 2011: Seasonal variation of surface temperature change during the last several decades. *J. Climate*, **24**, 3817–3821, doi:10.1175/JCLI-D-11-00129.1.

Matthewman, N. J., and G. Magnusdottir, 2011: Observed interaction between Pacific sea ice and the western Pacific pattern on intraseasonal time scales. *J. Climate*, **24**, 5031–5042, doi:10.1175/2011JCLI4216.1.

Melillo, J. M., T. C. Richmond, and G. W. Yohe, Eds., 2014: *Climate Change Impacts in the United States: The Third National Climate Assessment*. U.S. Global Change Research Program, 841 pp., doi:10.7930/J0Z31WJ2.

Mlawer, E. J., S. J. Taubman, P. D. Brown, M. J. Iacono, and S. A. Clough, 1997: Radiative transfer for inhomogeneous atmospheres: RRTM, a validated correlated-k model for the longwave. *J. Geophys. Res.*, **102**, 16 663–16 682, doi:10.1029/97JD00237.

Moore, G. W. K., 2012: Decadal variability and a recent amplification of the summer Beaufort Sea high. *Geophys. Res. Lett.*, **39**, L10807, doi:10.1029/2012GL051570.

Moritz, R. E., 1977: On a possible sea-breeze circulation near Barrow, Alaska. *Arct. Alp. Res.*, **9**, 427–431, doi:10.2307/1550535.

Muskett, R., 2012: Multi-satellite and sensor derived trends and variation of snow water equivalent on the high-latitudes of the Northern Hemisphere. *Int. J. Geosciences*, **3**, 1–13, doi:10.4236/ijg.2012.31001.

Overland, J. E., 2009: Meteorology of the Beaufort Sea. *J. Geophys. Res.*, **114**, C00A07, doi:10.1029/2008JC004861.

Parent, M. B., and D. Verbyla, 2010: The browning of Alaska's boreal forest. *Remote Sens.*, **2**, 2729–2747, doi:10.3390/rs2122729.

Pinzon, J. E., and C. J. Tucker, 2014: A non-stationary 1981–2012 AVHRR $NDVI_{3g}$ time series. *Remote Sens.*, **6**, 6929–6960, doi:10.3390/rs6086929.

Polyakov, I. V., U. S. Bhatt, J. E. Walsh, E. P. Abrahamsen, A. V. Pnyushkov, and P. L. Wassmann, 2013: Recent oceanic changes in the Arctic in the context of long-term observations. *Ecol. Appl.*, **23**, 1745–1764, doi:10.1890/11-0902.1.

Raynolds, M. K., D. A. Walker, H. E. Epstein, J. E. Pinzon, and C. J. Tucker, 2004: A vegetation map of the Arctic tundra biome (1:1, 750,000 scale): II. Analysis of the distribution of phytomass and vegetation types. *J. Veg. Sci.*, **3**, 403–411.

——, ——, ——, ——, and ——, 2012: A new estimate of tundra-biome phytomass from trans-Arctic field data and AVHRR NDVI. *Remote Sens. Lett.*, **3**, 403–411, doi:10.1080/01431161.2011.609188.

Santer, B. D., T. M. L. Wigley, J. S. Boyle, D. J. Gaffen, J. J. Hnilo, D. Nychka, D. E. Parker, and K. E. Taylor, 2000: Statistical significance of trends and trend differences in layer-average atmospheric temperature time series. *J. Geophys. Res.*, **105**, 7337–7356, doi:10.1029/1999JD901105.

Serreze, M. C., and A. P. Barrett, 2011: Characteristics of the Beaufort Sea high. *J. Climate*, **24**, 159–182, doi:10.1175/2010JCLI3636.1.

——, and R. G. Barry, 2011: Processes and impacts of Arctic amplification: A research synthesis. *Global Planet. Change*, **77**, 85–96, doi:10.1016/j.gloplacha.2011.03.004.

Shippert, M. M., D. A. Walker, N. A. Auerbach, and B. E. Lewis, 1995: Biomass and leaf-area index maps derived from SPOT images for Toolik Lake and Imnavait Creek areas. *Polar Rec.*, **31**, 147–154, doi:10.1017/S0032247400013644.

Shulski, M., and G. Wendler, 2007: *The Climate of Alaska.* University of Alaska Press, 216 pp.

Skamarock, W. C., and Coauthors, 2008: A description of the Advanced Research WRF version 3. NCAR Tech. Note NCAR/TN-475+STR, 113 pp. [Available online at http://www.mmm.ucar.edu/wrf/users/docs/arw_v3_bw.pdf.]

Steele, M., W. Ermold, and J. Zhang, 2008: Arctic Ocean surface warming trends over the past 100 years. *Geophys. Res. Lett.*, **35**, L02614, doi:10.1029/2007GL031651.

——, ——, and J. L. Zhang, 2011: Modeling the formation and fate of the near-surface temperature maximum in the Canadian basin of the Arctic Ocean. *J. Geophys. Res.*, **116**, C11015, doi:10.1029/2010JC006803.

——, S. Dickinson, J. Zhang, and R. Lindsay, 2015: Seasonal ice loss in the Beaufort Sea: Toward synchrony and prediction. *J. Geophys. Res. Oceans*, **120**, 1118–1132, doi:10.1002/2014JC010247.

Stegall, S. T., and J. Zhang, 2012: Wind field climatology, changes, and extremes in the Chukchi/Beaufort Seas and Alaska North Slope during 1979–2009. *J. Climate*, **25**, 8075–8089, doi:10.1175/JCLI-D-11-00532.1.

Sturm, M., C. Racine, and K. Tape, 2001: Climate change: Increasing shrub abundance in the Arctic. *Nature*, **411**, 546–547, doi:10.1038/35079180.

Takala, M., K. Luojus, J. Pulliainen, C. Derksen, J. Lemmetyinen, J.-P. Kärnä, J. Koskinen, and B. Bojkov, 2011: Estimating Northern Hemisphere snow water equivalent for climate research through assimilation of space-borne radiometer data and ground-based measurements. *Remote Sens. Environ.*, **115**, 3517–3529, doi:10.1016/j.rse.2011.08.014.

Tape, K., M. Sturm, and C. Racine, 2006: The evidence for shrub expansion in northern Alaska and the pan-Arctic. *Global Change Biol.*, **12**, 686–702, doi:10.1111/j.1365-2486.2006.01128.x.

Tewari, M., and Coauthors, 2004: Implementation and verification of the unified Noah land surface model in the WRF model. *Proc. 20th Conf. on Weather Analysis and Forecasting/16th Conf. on Numerical Weather Prediction*, Seattle, WA, Amer. Meteor. Soc., 11–15.

Treshnikov, A. F., 1985: *Atlas of the Arctic* (in Russian). Administrator of Geodesy and Cartography of the Soviet Ministry, 204 pp.

Tucker, C. J., 1979: Red and photographic infrared linear combinations for monitoring vegetation. *Remote Sens. Environ.*, **8**, 127–150, doi:10.1016/0034-4257(79)90013-0.

——, and P. J. Sellers, 1986: Satellite remote sensing of primary production. *Int. J. Remote Sens.*, **7**, 1395–1416, doi:10.1080/01431168608948944.

Urban, F. E., and G. D. Clow, 2014: DOI/GTN-P climate and active-layer data acquired in the National Petroleum Reserve–Alaska and the Arctic National Wildlife Refuge, 1998–2013. U.S. Geological Survey Data Series 892, accessed 24 January 2015, doi:10.3133/ds892.

Urban, M., M. Forkel, J. Eberle, C. Huttich, C. Schmullius, and M. Herold, 2014: Pan-Arctic climate and land cover trends derived from multi-variate and multi-scale analyses (1981–2012). *Remote Sens.*, **6**, 2296–2316, doi:10.3390/rs6032296.

Verbyla, D., 2008: The greening and browning of Alaska based on 1982–2003 satellite data. *Global Ecol. Biogeogr.*, **17**, 547–555, doi:10.1111/j.1466-8238.2008.00396.x.

Walker, D. A., 1985: Vegetation and environmental gradients of the Prudhoe Bay region, Alaska. U.S. Army Cold Regions Research and Engineering Laboratory CRREL Rep. 85-14, 237 pp.

——, W. D. Bilings, and J. D. De Molenaar, 2001: Snow-vegetation interactions in tundra environments. *Snow Ecology*, H. G. Jones et al., Eds., Cambridge University Press, 266–324.

——, and Coauthors, 2003: Phytomass, LAI, and NDVI in northern Alaska: Relationships to summer warmth, soil pH, plant functional types, and extrapolation to the circumpolar Arctic. *J. Geophys. Res.*, **108**, 8169, doi:10.1029/2001JD000986.

——, and Coauthors, 2005: The circumpolar Arctic vegetation map. *J. Veg. Sci.*, **16**, 267–282, doi:10.1111/j.1654-1103.2005.tb02365.x.

Wallace, J. M., and D. S. Gutzler, 1981: Teleconnections in the geopotential height field during Northern Hemisphere winter. *Mon. Wea. Rev.*, **109**, 784–812, doi:10.1175/1520-0493(1981)109<0784:TITGHF>2.0.CO;2.

Walsh, J. E., 1977: Measurements of the temperature, wind, and moisture distribution across the northern coast of Alaska. *Arct. Alp. Res.*, **9**, 175–182, doi:10.2307/1550579.

White, R. G., B. R. Thomson, T. Skogland, S. J. Person, D. E. Russell, D. F. Holleman, and J. R. Luick, 1975: Ecology of caribou at Prudhoe Bay, Alaska. *Ecological Investigations of the Tundra Biome in the Prudhoe Bay Region*, J. Brown, Ed., Biological Papers of the University of Alaska, Vol. 2, University of Alaska, 150–210.

Xu, L., and Coauthors, 2013: Temperature and vegetation seasonality diminishment over northern lands. *Nat. Climate Change*, **3**, 581–586, doi:10.1038/nclimate1836.

Yurtsev, B. A., 1994: Floristic division of the Arctic. *J. Veg. Sci.*, **5**, 765–776, doi:10.2307/3236191.

Zhang, T., 2005: Influence of the seasonal snow cover on the ground thermal regime: An overview. *Rev. Geophys.*, **43**, RG4002, doi:10.1029/2004RG000157.

——, T. E. Osterkamp, and K. Stamnes, 1996: Some characteristics of the climate in northern Alaska, U.S.A. *Arct. Alp. Res.*, **28**, 509–518, doi:10.2307/1551862.